6th International Conference on the Microscopy of Oxidation, April 4-6, 2005, University of Birmingham, UK, *to be publication in High Temp. Mater.* LBNL-57386

Stress Development and Relaxation in Al_2O_3 during Early Stage Oxidation of β-NiAl

P. Y. Hou[1], A. P. Paulikas[2] and B. W. Veal[2]

[1]Lawrence Berkeley National Laboratory
1 Cyclotron Rd. MS: 62-203
Berkeley, CA 94530

[2]Argonne National Laboratory
9700 S. Cass Ave.
Chicago, IL, 60439

Abstract

Using a glancing synchrotron X-ray beam (Advanced Photon Source, Beamline 12BM, Argonne National Laboratory), Debye-Scherrer diffraction patterns from thermally grown oxides on NiAl samples were recorded during oxidation at 1000 or 1100°C in air. The diffraction patterns were analyzed to determine strain and phase changes in the oxide scale as it developed and evolved. Strain was obtained from measurements of the elliptical distortion of the Debye-Scherrer rings, where data from several rings of a single phase were used. Results were obtained from α-Al_2O_3 as well as from the transition alumina, in this case θ-Al_2O_3, which formed during the early stage. Compressive stress was found in the first-formed transition alumina, but the initial stress in α-Al_2O_3 was tensile, with a magnitude high enough to cause Al_2O_3 fracture. New α-Al_2O_3 patches nucleated at the scale/alloy interface and spread laterally and upward. This transformation not only puts the alpha alumina in tension, but can also cause the transition alumina to be in tension. After a complete α-Al_2O_3 layer formed at the interface, the strain level in α-Al_2O_3 became compressive, reaching a steady state level around -75 MPa at 1100°C. To study a specimen's response to stress perturbation, samples with different thickness, after several hours of oxidation at 1100°C, were quickly cooled to 950°C to impose a compressive thermal stress in the scale. The rate of stress relaxation was the same for 1 and 3.5 mm thick samples, having a strain rate of ~$1x10^{-8}$/s. This behavior indicates that oxide creep is the major stress relaxation mechanism.

Introduction

It is well known that growth stresses develop in the oxide scale that forms on metals and alloys during high temperature oxidation [1]. The oxidizing component can relieve the stress by plastic deformation of the substrate [2], and/or by creep of the oxide [3]. Unrelieved growth stresses combined with thermal stresses that develop during cooling can initiate and drive scale failure. Knowing the development and magnitude of the growth stress not only provides for accurate modeling of scale or coating failure, but also facilitates understanding of the oxidation mechanism and the processes by which oxide structure is developed.

A few studies, in recent years, have followed in-situ the development of growth stresses in α-Al_2O_3 formed on NiAl using different X-ray diffraction techniques [4-7]. The data by Schumann et al [4] had a large error bar, about 200 MPa. Within this range, the growth stress, at 1100°C from 2-14 hrs, appeared constant about zero. Eisenreich et al [6] oxidized at 950°C and, following the stresses from 30-115 hrs, found an initial stress of -200 MPa (negative means it is in compression), which then increased to a steady state

level of 550 ±100 MPa. The measurements from Tortorelli et al [5], using a synchrotron source with high resolution and fast data acquisition capabilities, observed at 1100°C a high initial tensile stress that gradually decreased towards a steady state level of -150 MPa. This report agrees well with our preliminary results on NiAl where the growth stress was also determined in-situ using a synchrotron source but with a different acquisition and analysis technique [7].

The oxidation behaviors of NiAl, in terms of oxide growth rates, phases and microstructure changes, have been studied extensively. In summary, only Al_2O_3 is formed on β-NiAl at temperatures greater than 800°C. The first formed alumina is either the θ [8,9] or the γ phase [10]. These transition aluminas grow 1-2 orders of magnitude faster than α-Al_2O_3 [11], and the growth is mainly dominated by aluminum outward transport [12]. In the initially formed oxide, the oxide/alloy interface was found to be coherent [10] with a cube-on-cube orientation relationship with the alloy [10,8]. With further oxidation, randomly oriented α-Al_2O_3 particles nucleate at the scale/alloy interface and they form an incoherent interface with the alloy [10]. These nuclei eventually develop into a complete α-Al_2O_3 layer, while the initially formed γ and/or θ aluminas transform to the α phase with time; the transformation is faster at higher temperatures [13]. In all cases, the transition aluminas develop platelet like morphology. TEM analyses [14,15] have identified the plane of the platelets as (110), whether they are θ or γ-Al_2O_3; and the platelets are often heavily twinned along the [111] direction [15]. Surface smoothing of the platelets occurs with time as a spheroidization phenomenon driven by a reduction in surface energy [14].

Nucleation of the α-Al_2O_3 has also been studied using fluorescence spectroscopy [16,17], where the α and θ-Al_2O_3 phases within the scale can be easily detected and distinguished at room temperature. This technique does not reveal the vertical location of the phases within the scale, but has good lateral resolution. Results show that circular shaped α-Al_2O_3 islands nucleate in the scale, with higher density on rougher surfaces, and grow laterally by radial migration of the transformation front until they impinge. The kinetics of this process is logarithmic, unlike unconstrained θ-to-α transformation that follows a linear rate law [18]. The first formed α-Al_2O_3 (center of the islands) is the thinnest, because transition alumina growth is stopped earlier. Since there is ~5% volume shrinkage associated with this θ-to-α transformation, cracks are often observed in the oxide layer, and they form first at the center of the alpha islands. Ridges of oxides, which are associated with α-Al_2O_3 grain boundaries, develop and fill the cracks after the transformation is completed.

Although much is known about the alumina transformation process during initial stage oxidation of NiAl, there has not been work done on the stress development in the different aluminas. Furthermore, since most stress studies to date show a steady stage growth stress level not more than 200 MPa, effective stress relaxation processes must exist during oxidation. It is therefore the intent of this work to i) follow the stresses in α as well as in transition aluminas as a function of oxidation time, in order to relate the stresses to the changes in oxide phases and morphology, and ii) study the rate of stress relaxation to determine the mechanism that is involved in relieving the oxidation stresses.

Experimental

In-situ strain measurements were performed using x-ray diffraction (XRD) exploiting synchrotron radiation at beamline 12BM at the Advanced Photon Source at Argonne National Laboratory. Details of the experimental setup have been described

elsewhere [7]. A test sample is placed in an open-ended horizontal tube furnace, where a 21.6 keV x-ray beam, with a spot size of about 0.1 mm (FWHM) x 1 mm, strikes the sample surface at an incidence angle of 2 to 5°. Half circles of Debye-Sherrer diffraction rings from the sample are recorded using an image plate detector. For precise determination of the x-ray scattering center, or any detector misorientation, a porous, sintered alumina is used as a reference. The reference is placed into the x-ray path, using a pneumatic actuator, after the test specimen is lowered. The x-rays penetrate through this thin reference and yield full-circle diffraction spectra that can be analyzed to obtain the location of the beam centroid to within ± 2 μm. The reference and sample motions are computer driven; typically, a reference spectrum is recorded after five successive sample measurements, each of 5 minutes duration.

The technique is a single exposure method, where diffraction rings from all diffracting planes in the accessible range of ψ (~ 7 - 75^o) are simultaneously acquired, where ψ is the angle between the sample normal and the scattering vector. Since in-plane and out-of-plane d-spacings of diffracting planes in a stressed film are different, the resulting Debye-Scherrer rings are elliptically distorted. This ellipticity is measured and analyzed to determine the strain in the film, while the oxide film is assumed to be isotropic with no shear and is under a biaxial stress. Slurries of Al_2O_3 powders applied on different substrates have been used as test samples up to 1100^{o}C to verify the position of zero strain. Four such tests have been run and the results show a zero strain level within ±20 MPa.

Test specimens, Ni-40Al and Ni-55Al (all in atomic percent), were cut from ~ 1 cm diameter rod-shaped ingots made by induction melting of high purity Ni and Al powders and homogenized in vacuum at 1150^{o}C for 15 hours. The alloy grain size ranged from 220-3200 μm, with an average of 590 μm. Specimens were cut perpendicular to the rod into 1 mm or 3.5 mm thick discs. The sample surface was polished to a 1 μm finish with diamond paste. After the test sample was carefully positioned in the path of the X-ray beam, it was heated at a linear rate to the oxidation temperature of 1000 or 1100^{o}C at a rate of 1000^{o}C/hr in ambient air. Diffraction patterns were recorded after the sample reached its desired oxidation temperature at 5 min intervals during the isothermal stage and continuing through cool down. All samples were furnace cooled, reaching near ambient temperature in about 1 hr. Two Ni40Al samples with different thicknesses were subjected to a sudden temperature change after a period of isothermal oxidation. The temperature at 1100^{o}C was reduced and held at 950^{o}C to examine the build up and relaxation of thermal stresses. After the strain study, test samples were examined using conventional x-ray diffraction and scanning electron microscopy. Duplicate specimens oxidized under the same conditions elsewhere were used to reveal the morphological development of the oxide scales. In order to examine the morphology at the scale/alloy interface and the scale in cross-section, part of the oxide scale was removed [19] by pulling on a 3 mm diameter stub that was glued onto the sample surface.

Results and Discussions

Alumina Strains on Ni-55Al at 1000^{o}C and 1100^{o}C

Changes in strain and intensity as determined from different alumina reflections on Ni-55Al at 1000^{o}C are shown in Figure 1. Time zero was taken as the time when temperature reached 1000^{o}C from a heating rate of 1000^{o}C/hr. The average strain for α-Al_2O_3 was determined from its (116), (024) and (113) rings, but only the weakest (012) intensity was used to show the amount of α-Al_2O_3 in the scale. The intensities are not normalized, so the trend, not the magnitude, should be used to indicate the development of

different alumina phases in the growing oxide. Two transition alumina rings were analyzed: the more intense one had a d-spacing of 2.71 Å and the less intense one of 1.90 Å. The former lattice parameter matched closely with that of the (202) and/or (002) planes and the latter to the (112) planes of θ-Al_2O_3. None of them matched γ-Al_2O_3. The small difference in strain between the two theta rings is believed to be due to elastic anisotropy, which we often observe on different reflections after cool down. Also, the (112) ring is very weak, hence the strain data are noisy and are probably less accurate.

The strain level in α-Al_2O_3 was tensile for the entire 12 hrs of oxidation, and the level continued on a downward trend towards zero. Using an oxide modulus of 360 GPa, an average of published values [20], the highest stress level for α-Al_2O_3 would be 460 MPa. Both reflections of θ-Al_2O_3 were present at time zero and remained detectable for the entire duration of the oxidation run, but the low intensity and heavy texture of the 1.90 Å ring prohibited reliable strain analysis during the first 6-7 hrs. The transition alumina intensities started to decrease after 9 hrs, while α-Al_2O_3 intensity increased rapidly. The strains in the theta alumina were compressive, relaxing toward zero as oxidation proceeded. The elastic modulus for θ-Al_2O_3 is unknown, but may be close to that of the spinel $MgAl_2O_4$ [21], which has E=241 GPa. Using this value, the maximum compressive strain in the θ-Al_2O_3 would be -480 MPa.

Figure 2 is similar to Figure 1, but shows the data for Ni-55Al oxidized at 1100^{o}C; the lack of data points between 2-3 hrs was due to a temporary synchrotron beam loss. At this higher temperature, transformation to α-Al_2O_3 was much faster, as expected. θ-Al_2O_3 was only detected within the first 2 hrs. The α-Al_2O_3 started in high tension, but this level gradually decreased to zero after about 4 hrs. It is seen that relaxation of the stress in θ-Al_2O_3 is faster than that in alpha, and compressive stress built up in α-Al_2O_3 long after the θ-Al_2O_3 had transformed. At the end of the test run, the stress level in α-Al_2O_3 was only -72 MPa and it seemed to be reaching a steady state level where stress generation and relaxation processes are at equilibrium with one another.

Using the theta (202) intensity maximum as a marker, Fig. 3 compares the strain and intensity developments at the two temperatures, and it is seen that their behaviors are basically the same. This indicates that the higher temperature accelerates the kinetics of transformation and scale growth, but does not change the mechanisms.

Alumina Scale Development on Ni-55Al

Using Fig. 3 as a guide, scale morphology at different stages of the stress development, marked by A, B and C on the figure, was observed from specimens oxidized for different times. Initially, at location A, patches of α-Al_2O_3 imprints could be seen at the alloy surface after scale removal (Fig. 4). This observation is in agreement with previous TEM cross-sections [10,22], which found α-Al_2O_3 nucleates at the transition alumina/alloy interface. The first-formed alpha patches are circular in shape and boundaries are naturally formed as they impinge onto each other. Their numbers, but not sizes, vary significantly on different alloy grains, and preferential nucleation took place on scratch marks. Matching microstructures, i.e., patches of circular shaped oxides mixed within a fine grained scale, were also found on the underside of the oxide scale; an example is shown in Fig. 4c. Fine particle-like features, less than 250 nm in diameter, are seen everywhere on the underside. Their composition and origin are not yet known, but are believed to be contaminants that came from the pull test.

Figure 5a shows a magnified view of the imprints made by two of these circular patches. Both are about 5 μm in diameter; one has broken up into 3 grains, from what appears to be radial cracks, and the other is still single-grained, but with facets of some preferred orientations. Corresponding grooves of these radial cracks were also found on the underside of the oxide; they can be seen on some of the patches in Fig. 4c. Since the first-formed alpha grains were under as much as 460 MPa tensile stress, and the fracture stress for alumina is only 100 MPa for a critical defect size of 1 μm [23], fracture is indeed expected. On the oxide surface, dense grain areas with similar but slightly smaller sizes than the alpha patches found at the interface are everywhere; a magnified view of one is shown in Fig. 5b. According to Tolpygo and Clarke [17], these are areas above the first transformed α-Al_2O_3. However, at this early stage, cracks could not be detected. Maybe they are too fine to be discerned in the midst of the many platelets surrounding the areas, or maybe the α-Al_2O_3 has not yet transformed through the entire thickness of the scale. From Figure 6, it is seen that the θ-Al_2O_3 was tri-layered with a very fine grained dense layer adjacent to the alloy, followed by an intermediate layer filled with fine platelets and ending with a surface layer of large, loosely packed platelets. The first transformed circular patches covered the entire thickness of the dense inner layer, but do not appear to have extended all the way through the intermediate layer. This seems to suggest that the transformation front extends faster laterally than vertically, since the patches are about 5 μm in diameter, but the inner theta layer is only about 0.5 μm thick.

At a later stage, location B on Fig. 3, α-Al_2O_3 grain imprints were found to cover about 80% of the alloy surface (Fig. 7a). Cracks could now be observed at some locations on the scale surface (Fig. 7b), and they often have similar morphology as those seen on the bottom of the α-Al_2O_3 patches (Fig. 5), indicating that these cracks had run through the entire thickness of the alpha grains. After an even longer time, point C on Fig. 3, transformation to alpha was complete, even though platelets continue to be present on the oxide surface (Fig. 8a). Cracks are still seen on the scale surface with new oxides that look like ridges forming within them. The entire alloy surface was covered with α-Al_2O_3 grain imprints. The α-Al_2O_3 grain size (as seen in Fig. 8b) is on average smaller that that seen on Fig. 6a. This is because cracking of the initial large alpha patches has made new grains.

Stress Relaxation

Two Ni-40Al samples with 1 mm and 3.5 mm thickness, respectively, were measured at 1100^{o}C. To observe the rate of stress relaxation, each test sample was quickly cooled to 950^{o}C after 6 or 7 hours of oxidation at 1100^{o}C. This temperature drop induced a compressive stress in the oxide, which arose from the thermal expansion mismatch between the oxide and the alloy, and its relaxation was followed for 3 to 4 hours before raising the temperature up to 1100^{o}C again. The average strain levels in α-Al_2O_3 observed during these temperature excursions are shown in Fig. 9a for the two samples. Similar to that found on the Ni-55Al, the α-Al_2O_3 was initially in tension. However, the stress dropped to compression much faster on the 3.5 mm sample. This behavior indicates a faster θ-to-α transformation rate, which is likely caused by a grain orientation effect, since alloy grain orientation can affect nucleation rates (as seen in Fig. 4) and these alloys tend to have unusually large grains on which the x-ray beam could fall. As soon as the temperature was brought back to 1100^{o}C (at ~ 12 hrs), the compressive stress started to build up in the oxide, and eventually reached the steady-state level that existed before the

temperature interruption. This behavior clearly indicates that compressive growth stresses are generated as α-Al_2O_3 grows.

The relaxation observed at 950°C could be due to oxide or alloy deformation, or both. The strain rates for the 1 and 3.5 mm thick samples are 1.06 and 1.18×10^{-8}/s respectively. The two values are very similar, indicating no effect of substrate thickness. Since $\sigma_m = \sigma_{ox}(2h_{ox}/h_m)$, where σ's are the stresses and h's the thicknesses of the metal and the oxide, taking the maximum thermal stress induced by lowering the temperature from 1100 to 950°C to be -500 and -350 MPa respectively for the 1mm and the 3.5 mm samples, and an oxide thickness at this time to be 1μm, according to our kinetics data, the stress level in the 1 mm and the 3.5 mm thick substrates should be 1 and 0.2 MPa respectively. Deformation of coarse grained NiAl (average grain size of 170 μm) occurs by dislocation-dominated processes [24], where at 1027°C the strain rate under 1 MPa would be 2×10^{-11}/s, which is three orders of magnitude lower than our measured rate at 950°C. Earlier studies of β-NiAl deformation [25] included data at 950°C on alloys having an average grain size of ~500 μm. The strain rates at 1 and 0.2 MPa are expected to be, respectively, 5×10^{-9} and 3×10^{-11}/s. Although these values are much higher than that reported by Arzt and Grahle [24], probably due to higher alloy purity [25], the expected deformation rate due to alloy deformation is still 3 orders of magnitude lower than our result on the 3.5 mm thick sample, where the level of stress in the alloy is only 0.2 MPa. Therefore, the relaxation observed in this work must have occurred within the fine-grained oxide scale.

No deformation studies of α-Al_2O_3 have been conducted at temperatures as low as 950°C. From the data of Cannon et al [26] (1×10^{-5} to 1×10^{-3}/s between 1192-1418°C), and of Lin and Becher [27] (3×10^{-5} and 4×10^{-6}/s respectively at 1200 and 1300°C), the strain rate at 950°C, extrapolated from a strain rate vs. 1/temperature plot, is 1×10^{-8}/s, which agreed extremely well, perhaps to a certain extent by chance, with our result. The average alumina grain size in these studies was 1.2 and 2 μm respectively, which is similar to that of the thermally grown α-Al_2O_3 after cracking from the initially formed circular patches. A good representation of the α-Al_2O_3 grain size can be seen in Fig. 8b.

When ln (absolute strain) at 950°C is plotted against time, Fig. 9b, the data points can be fitted to a linear curve, indicating the following relationship $d\varepsilon/dt = -A\sigma^n$ with a stress exponent of one, as in the case of diffusional creep under low stresses [28]. If this were true, one would expect Coble creep to be responsible, due to the small grain size and the low temperature. Since creep rate, $\dot{\varepsilon}$, is controlled by the slower diffusing specie along the fastest path, generally considered to be Al transport through grain boundaries, one can write an approximate creep equation [29]:

$$\dot{\varepsilon} = \frac{14\Omega\sigma}{kTd^3}\left(\frac{\pi\delta D_b^{Al}}{d}\right)$$

where Ω is the atomic volume of α-Al_2O_3, δD_b^{Al} the grain boundary diffusivity of Al, d the grain size and σ the applied stress. Extrapolating from δD_b^{Al} values complied from creep studies by Cannon and Coble [29], $\dot{\varepsilon}$ at 950°C for d=1μm is ~2×10^{-7}/s, which is an order of magnitude higher than that reported here. If the tracer diffusivity, D_b^{Al}, from Paladino and Kingery [30] is used, assuming a grain boundary width, δ, of 10^{-7} cm, the creep rate becomes $1\text{x}10^{-10}$/s, which is 100 times slower than our measured rate. Since published grain boundary diffusivity measurements for Al are highly uncertain [31], we are unable,

at this time, to satisfactorily test the validity of the Coble model. Adding to the difficulty is the fact that diffusivity data are not available at the low temperatures investigated in these experiments and must be extrapolated. The mechanism of deformation, therefore, is not yet certain.

Mechanism of Al_2O_3 Transformation in Relation to Stress Development

Based on the results presented so far, the mechanism of Al_2O_3 development on NiAl can be further understood as follows. Initially, a thin, dense and fine-grained transition alumina forms on the alloy with compressive stresses at least as high as -480 MPa. Since previous TEM works [8,10] have shown that the initial oxide formed epitaxially, and we also observe strong texture on the theta rings, the first-formed theta most likely grew epitaxially with an associated epitaxial stress. It seems that when the temperature is lower than 1000°C, the transition alumina is γ-Al_2O_3 [10,22,32], but above 1000°C, it is in the form of θ-Al_2O_3. This is in agreement with theoretical thermal stabilities of various transition aluminas [33], where the stability increases with temperature from γ-Al_2O_3, δ-Al_2O_3, θ-Al_2O_3 to α-Al_2O_3. Above 1000°C, α should be the most stable form, but transformation from γ or θ to α is limited by the nucleation step. Preferential nucleation took place on alloy scratch marks, and the process also depends strongly on alloy grain orientation.

The first α-Al_2O_3 nucleates at the scale/alloy interface. It is important to realize that this is mainly due to alumina transformation instead of new inward oxide growth, because the first formed α was always in high tension (Figs. 1 and 2), which resulted from the volume contraction associated with the transformation process. The transformation front then extends laterally in the radial direction and upward through the θ layer and the rate of extension is faster laterally than upward.

When the transformed α patches begin to grow in a compressed θ layer with an associated volume contraction, the compression in the θ layer is relaxed, and this relaxation process continues as new alpha patches are formed and the initial ones grow. Depending on the level of the initial compressive stress and the rate by which it is relieved from the $\theta \rightarrow \alpha$ volume contraction, there may be a time when all the initial compression is relaxed and the θ film is put under tension, as with the Ni55Al oxidized at 1100°C (Fig. 2). Stress relaxation in θ was faster than that in the transformed α (Figs. 1 and 2). Relaxation of the compressive stress and subsequent buildup of tensile stress in θ-Al_2O_3 can be accomplished in the transformation process with no new scale growth. In the absence of new growth, the stress in the α-Al_2O_3, resulting from the conversion process, will be tensile. When the phase transformation is completed, the continued decrease of the tensile stress and the eventual build up of a compressive stress in α-Al_2O_3 must come from creep relaxation and new oxide growth with its associated compressive growth stress.

When the tensile stress cannot be quickly relaxed by the surrounding scale, cracks can develop and that is seen here and has been observed by many others [8,9,17,32]. While all others have observed these cracks on the oxide surface, similar to those shown in Figs. 7b and 8a, our results also show them at the base of the transformed α-Al_2O_3. It should also be noted that cracking only occurred in large, single grained α-Al_2O_3 patches that are most likely not able to creep. Although surface cracks are easier to nucleate, cracks can also nucleate within the scale and eventually penetrate through the entire scale thickness, allowing oxygen ingress to the alloy surface, followed by new α-Al_2O_3 growth to fill the cracks. Although the number of α nuclei may dictate the final α-Al_2O_3 grain

size [17], cracking can also break up the growing α-Al_2O_3 patches to create new grains, leading to crack-filling ridges on α grain boundaries.

Initial tension in α-Al_2O_3 was not found on FeCrAl [7]. This is because Fe_2O_3 and Cr_2O_3 are present in the very early stages and they acted as templates for α-Al_2O_3 nucleation [34]. Unlike NiAl, the first formed fine grained scale on FeCrAl consisted not only of transition alumina, but also α-Al_2O_3 [22]. These α grains, being embedded in the first-formed thin layer, were under a compressive stress of -400 MPa, and similar situations exist for Fe-28Al [7,35]. The high initial compressive stress also relaxed quickly to a steady state level of -40 MPa. Indicating again a condition where the stress generation and relaxation processes are in equilibrium.

Compressive strain in α-Al_2O_3 continues to build up after the transformation process is complete. This must be due to the presence of a compressive growth stress associated with alpha alumina growth. Since the sample is under an oxidizing environment, the first formed α would undoubtedly grow as a result of oxidation as well as transformation, although the latter process has a much higher rate.

Conclusions

- At 1000 and 1100^{o}C, in air, θ-Al_2O_3 forms initially on NiAl with a three-layered structure: a dense, fine-grained inner layer, a fine platelet filled intermediate layer and an outer layer containing loosely packed large platelets. The first formed θ-Al_2O_3 was under a high compressive stress of at least -480 MPa.
- α-Al_2O_3 nucleates in the transition alumina at the oxide/alloy interface. Nuclei are formed preferentially along alloy scratch marks, and the nucleation rate depends on alloy orientation. Transformed α-Al_2O_3 patches grew laterally and through the thickness of the θ layer. The rate is faster laterally than through scale.
- The first formed α-Al_2O_3, due to volume contraction from the transformation process, is under 400-500 MPa tensile stress, causing scale cracking. As transformation continues, the level of tensile stress in the α phase and compressive stress in the θ phase both decrease towards zero. Depending on the relative magnitude of the two stresses and the relaxation processes, the θ phase can also be in tension towards the end of the transformation.
- Compressive stress is associated with α-Al_2O_3 growth as the stress level continues to build up after the alumina phase transformation is complete. At steady state, the stress level in α-Al_2O_3 is only -75 MPa at 1100^{o}C due to an equilibrium between stress generation and relaxation processes.
- Thermally induced stresses in the α-Al_2O_3 scale are effectively relaxed in the oxide layer. The strain rates under –(500-250) MPa for alloy-to-scale thickness ratios of 1000 and 3500 are both in the range of $(1.12\pm0.06)\times10^{-8}$/s.

Acknowledgment

Research sponsored by the U. S. Department of Energy, BES, Materials Science, under contracts No. DE-AC03-76SF00098 and W-31-109-ENG-38.

References

1. See for example the review by Stringer, J. Stress generation and relief in growing oxide films. *Corr. Sci*., **10**, 513-543 (1970).

2. Evans, H.E. and Taylor, M.P. Creep relaxation and the spallation of oxide layers. *Surf. Coatings Tech*. **94-95**, 27-33 (1997).

3. Schutze, M. Plasticity of protective oxide scales. *Mater. Sci. Tech*., **6**, 32-38 (1990).

4. Schumann, E., Sarioglu, C., Blachere, J.R., Pettit, F.S. and Meier, G.H. High-temperature stress measurements during the oxidation of NiAl. *Oxid. Metals*, **53**, 259-472 (2000).

5. Tortorelli, P.F., More, K.L., Specht, E.D., Pint, B.A. and Zschack, P. Growth stress-microstructure relationships for alumina scales. *Mater. at High Temp,* **20**,303-310 (2003).

6. Eisenreich, N., Fietzek, H., Garcia-Vargas, M.J., Juez-Lorenzo M. and Kolarik, V. In situ investigation of kinetics and stresses in alumina scales on NiAl during the phase transformation theta to alpha. *J. Corr. Sci. Eng*., **6,** H062 (2003).

7. Hou, P.Y., Paulikas, A.P. and Veal, B.W. Growth strains and stress relaxation in alumina scales during high temperature oxidation. *Mater. Sci. Forum* **461-464**, 671-680 (2004).

8. Doychak, J., Smialek J.L. and Mitchell T.E. Transient oxidation of single-crystal β-NiAl. *Met. Trans. A* **20A**, 499-518 (1989).

9. Rybicki, G.C. and Smialek, J.L. Effect of the θ–α-Al_2O_3 transformation on the oxidation behavior of β-NiAl+Zr. *Oxid. Metals* **31**, 275-304 (1989).

10. Yang, J.C., Nadarzinski, K., Schumann, E. and Rühle, M. Electron microscopy studies of NiAl/γ-Al_2O_3 interfaces. *Scripta Met.* **33**, 1043-48 (1995).

11. Brumm M.W. and Grabke, H.J. The oxidation behaviour of NiAl. I. phase transformations in the alumina scale during oxidation of NiAl and NiAl--Cr Alloys. *Corr. Sci.*, **33**, 1677-1690 (1992).

12. Prescott, R., Mitchell, D.F. and Graham, M.J. A study of the growth of α-Al_2O_3 scales using high-resolution imaging secondary ion mass spectrometry, *Corr.*, **50**, 62-71 (1994).

13. Doychak J. and Ruhle, M. TEM Studies of oxidized NiAl and Ni_3Al cross sections, *Oxid. Met*. **31**, 431-452 (1989).

14. Doychak, J.K. Doctoral thesis, Case Western Reserve University, Cleveland, Ohio (1986).

15. Yang, J.C. Schumann, E. Levin I. and Rühle, M. Transient Oxidation of NiAl", *Acta Metall*, **46**, 2195-2201 (1998).

16. Lipkin, D.M. Schaffer, H. Adar F. and Clarke, D.R. Lateral growth kinetics of α-alumina accompanying the formation of a protective scale on (111) NiAl during oxidation at 1100^{o}C, *Appl. Phys. Lett*., **70**, 2550-2552 (1997).

17. Tolpygo V.K. and Clarke, D.R. Microstructural study of the theta-alpha transformation in alumina scales, *Mater. High Temp.*, **17**, 59-70, (2000).

18. Steiner, C.J.-P. Hasselman D.P.H. and Spriggs, R.M. Kinetics of the gamma-to-alpha alumina phase transformation, *J. Am. Ceram. Soc.* 412-413, (1971).

19. Hou P.Y. and Priimak K. Interfacial segregation, pore formation and scale adhesion on NiAl alloys. *Oxid. Metals* **63**, 113-130 (2005).

20. The Oxide Handbook, Second Edition, p. 183, ed. G. V. Samsonov, IFI/Plenum, New York, 1982.

21. Li, C., Ohmori, A., McPherson, R., The relationship between microstructure and Young's modulus of thermally sprayed ceramic coatings, *J. Mater. Sci*., **32**, 997-1004 (1997).

22. Andoh, A., Taniguchi, S. and Shibata, T. TEM observation of phase transformations of alumina scales formed on Al-Deposited Fe-Cr-Al foils, *Mater. Sci. Forum*, **369-372**, 303-310, (2001).

23. Schutze, M., Failure of oxide scales on advanced materials due to the presence of stresses, *Proc. workshop high temperature corrosion of advanced materials and protective coatings*, ed., Y. Saito, B. Onay and T. Maruyama, pp. 39-49, Elsevier Sci. Pub. (1992).

24. Arzt, E. and Grahle, P. High temperature creep behavior of oxide dispersion strengthened NiAl intermetallics. *Acta mater*. **46**, 2717-2727 (1998).

25. Vandervoort, R.R., Mukherjee, A.K. and Dorn, J.E. Elevated-temperature deformation mechanisms in β-NiAl, *Trans ASM*, **59**, 930-944 (1966).

26. Cannon, R.M., Rhodes, W.H. and Heuer, A.H. Plastic deformation of fine-grained alumina (Al_2O_3): I. Interface-controlled diffusional creep, *J. Am. Cerem. Soc*., **63**, 46-55 (1980).

27. Lin, H-T. and Becher, P.F. Creep behavior of a SiC-whisker-reinforced alumina, *J. Am. Cerem. Soc.*, **73**, 1378-81 (1990).

28. Kingery, W.D., Bowen, H.K. and Uhlmann, D.R., Introduction to Ceramics, second edition, p. 736, Wiley-Interscience, New York, 1975.

29. Cannon R.M. and Coble R.L. Review of diffusional creep of Al_2O_3, in *Deformation of Ceramic Materials*, ed. R. C. Bradt and R. E. Tressler, Plenum Press, N.Y., pp. 61-100 (1975)

30. Paladino, A.E. and Kingery W.D. Aluminum ion diffusion in aluminum oxide, *J. Chem. Phy.*, **37**, 957-962 (1962).

31. Cannon, R.M. and Hou, P.Y., Diffusion induced stress generation during oxidation, in *"High Temperature Corrosion and Materials Chemistry"*, ed. P. Y. Hou, M. J. McNallan, R. Oltra, E. J. Opila and D. A. Shores, pp. 594-607, the Electrochem. Soc., 1998.

32. El Kadiri, H, Molins, R. and Bienvenu, Y. Phase transformation and growth of alumina on a thin FeCrAl-RE foil at around 900^{o}C, *Mater. Sci. Forum*, **461-464**, 1107-1116 (2004).

33. Mosely, P.T., Hyde, K.R., Bellany, B.A. and Tappin, G. The microstructure of the scale formed during the high temperature oxidation of a Fecralloy steel. *Corros. Sci.* **24**, 547- (1984).

34. Renusch, D., Grimsditch, M., Koshelev, I., Veal, B.W. and Hou, P.Y. Strain determination in thermally-grown alumina scales using fluorescence spectroscopy, *Oxid. Met.*, **48**, 471-495 (1997).

35. Zhang, X.F., Thaidigsmann, K., Ager, J. and Hou, P.Y., Initial stage Al_2O_3 scale development on iron aluminides, manuscript in preparation.

Figure Captions

Figure 1: Development of (a) strain and (b) intensity as determined from alpha reflections and two transition alumina reflections on Ni-55Al oxidized at 1000°C. The d-spacings of transition aluminas are expressed in angstroms. The strain level in α-Al_2O_3 is averaged from its (116), (024) and (113) rings.

Figure 2: Similar to Fig. 1, but on Ni-55Al oxidized at 1100°C.

Figure 3: Comparison of the strain and intensity developments in aluminas on Ni55Al at (a) 1100°C and (b) 1000°C. Locations marked by A, B and C are conditions where scale morphologies are observed.

Figure 4: SEM images showing the alloy surface and oxide underside after scale removal. (b) is the specimen surface under a pull stub showing partial failure at the scale/alloy interface exposing two large alloy grains. (a) and (d) are magnified views from grains 1 and 2 respectively, showing different number density of α-Al_2O_3 patches, patch impingement and preferential patch formation along scratch marks. (c) is an image from the underside of the oxide after pulling; small particle like features may be contaminants.

Figure 5: SEM images of (a) two α-Al_2O_3 patches on the alloy surface and (b) platelets and a finer grained patch on the oxide surface.

Figure 6: SEM images of (a) fractured scale cross-section showing three structurally different layers of θ-Al_2O_3. (b) Magnified view of the intermediate layer consists of fine, dense platelets. (c) Fractures at oxide/alloy and inner/intermediate layer interfaces showing transformed patches through the inner layer. (d) Magnified view of (c) showing the grain structure above a transformed patch.

Figure 7: SEM micrographs of scales after the end of the 1000°C strain test, showing (a) scale cross section showing α-Al_2O_3 throughout the inner layers of the first formed theta and large alpha imprints on the alloy. (b) Oxide surface with platelets, dense grained areas and cracks.

Figure 8: SEM micrographs of scale after the end of the 1100°C strain test, showing (a) surface oxide with platelets, cracks and oxide ridges filling the cracks, and (b) scale x-section and the α-Al_2O_3 imprinted alloy surface.

Figure 9: (a) Average strain in α-Al_2O_3 formed on 1 mm and 3.5 mm thick Ni-40Al oxidized at 1100°C, then reduced to 950°C for strain relaxation studies. (b) The change in strain with time at 950°C for the two samples with different substrate thickness; solid lines are linear fits to the data.

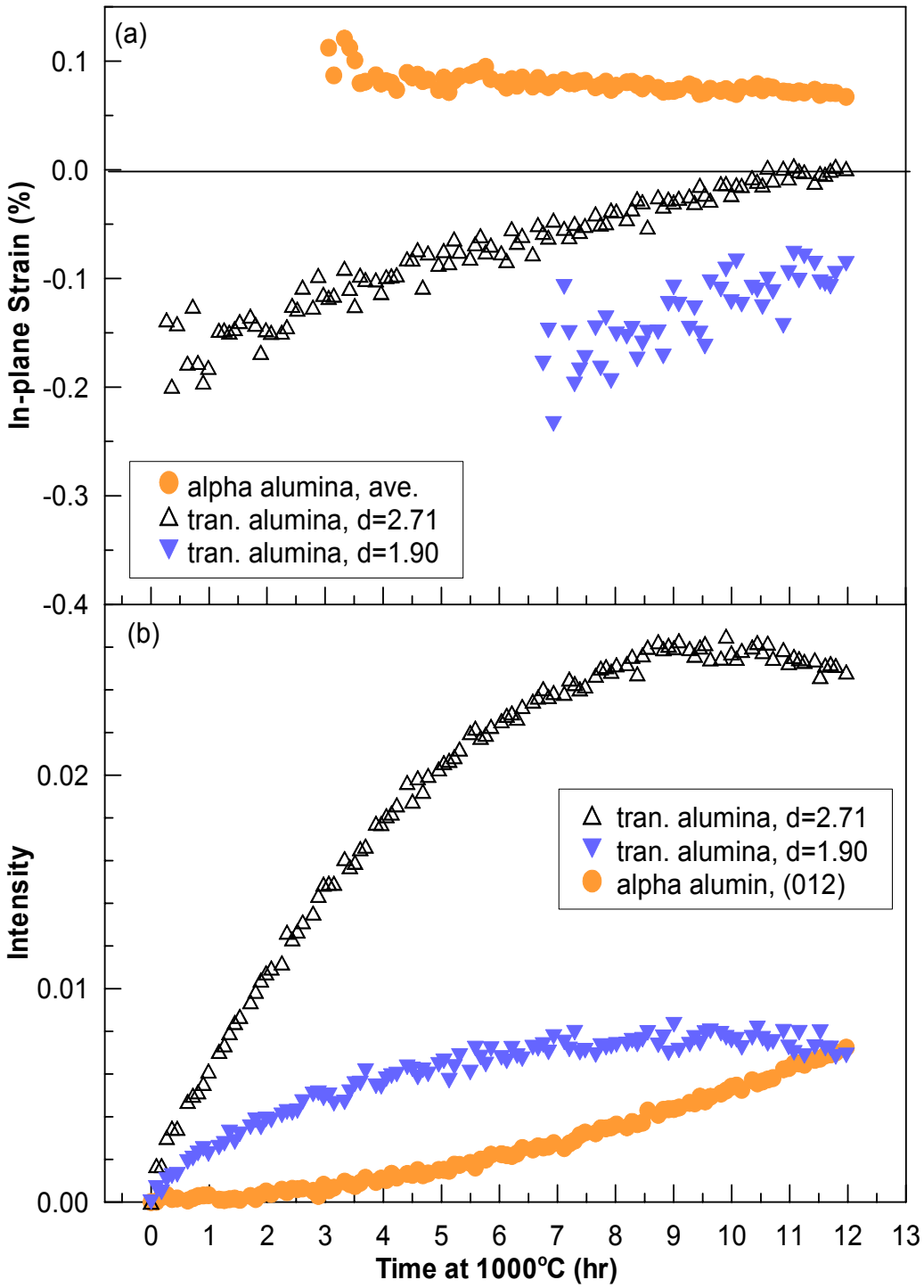

Figure 1: Development of (a) strain and (b) intensity as determined from alpha reflections and two transition alumina reflections on Ni-55Al oxidized at 1000°C. The d-spacings of transition aluminas are expressed in angstroms. The strain level in α-Al_2O_3 is averaged from its (116), (024) and (113) rings.

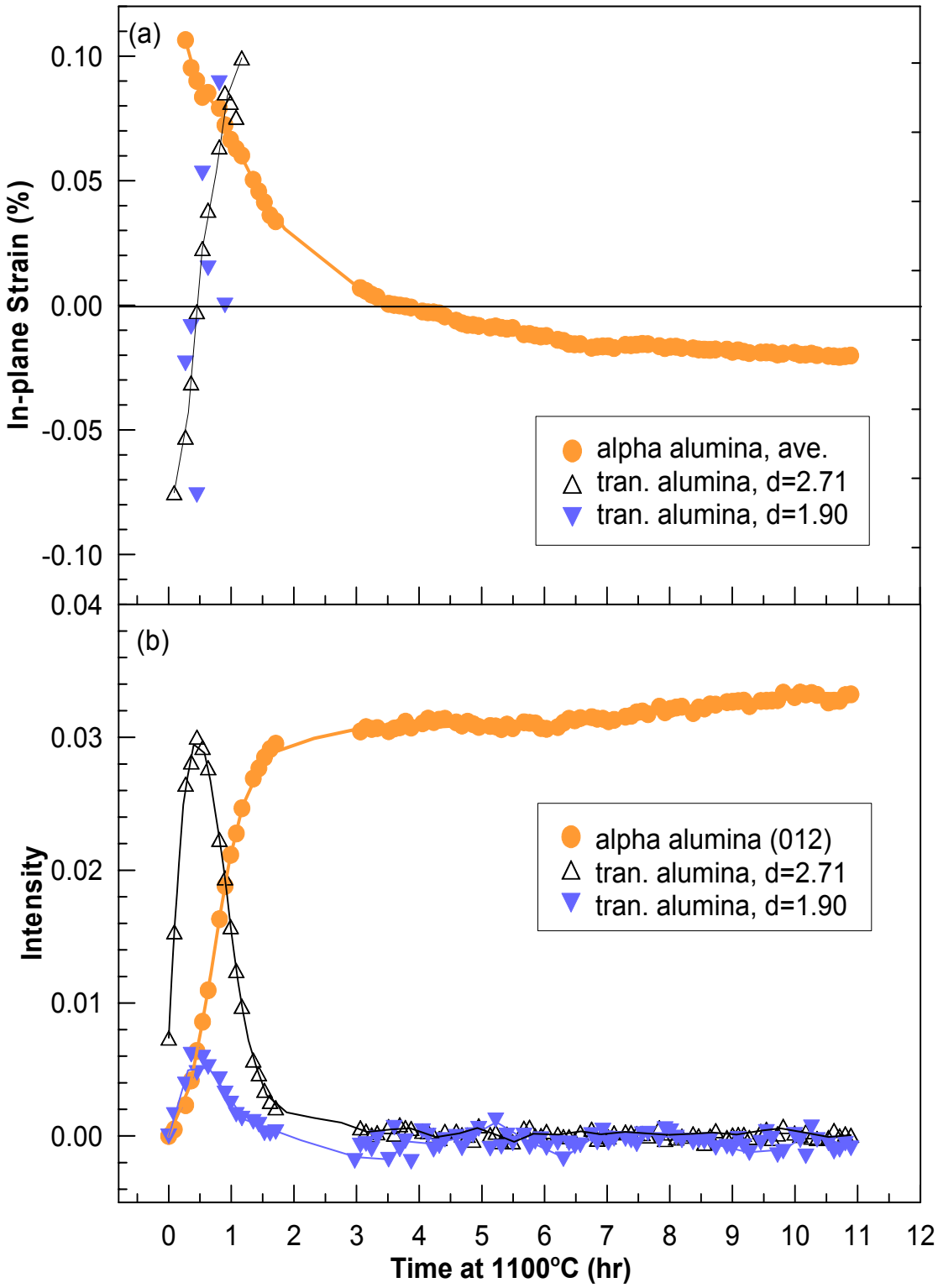

Figure 2: Similar to Fig. 1, but on Ni-55Al oxidized at 1100°C.

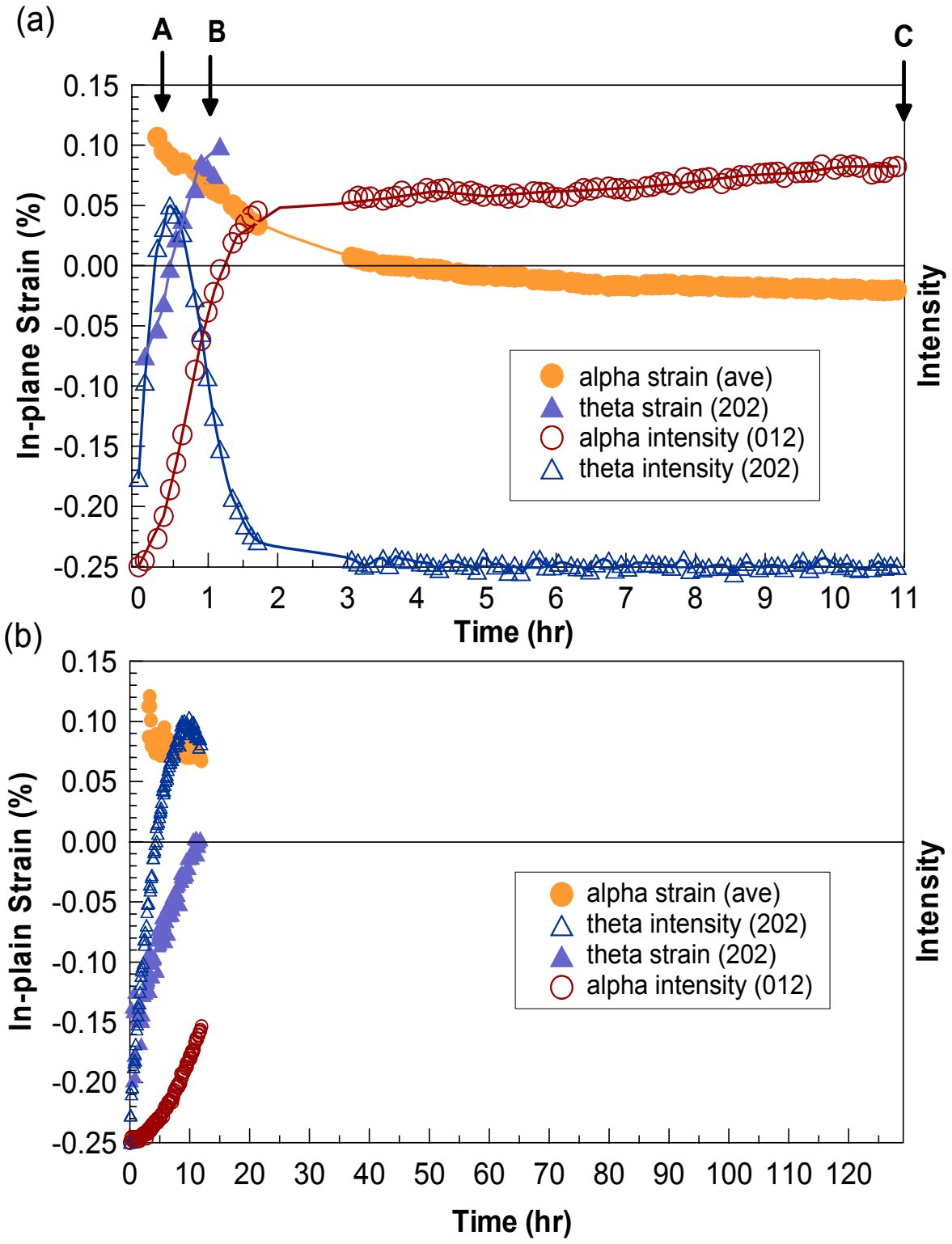

Figure 3: Comparison of the strain and intensity developments in aluminas on Ni55Al at (a) 1100°C and (b) 1000°C. Locations marked by A, B and C are conditions where scale morphologies are observed.

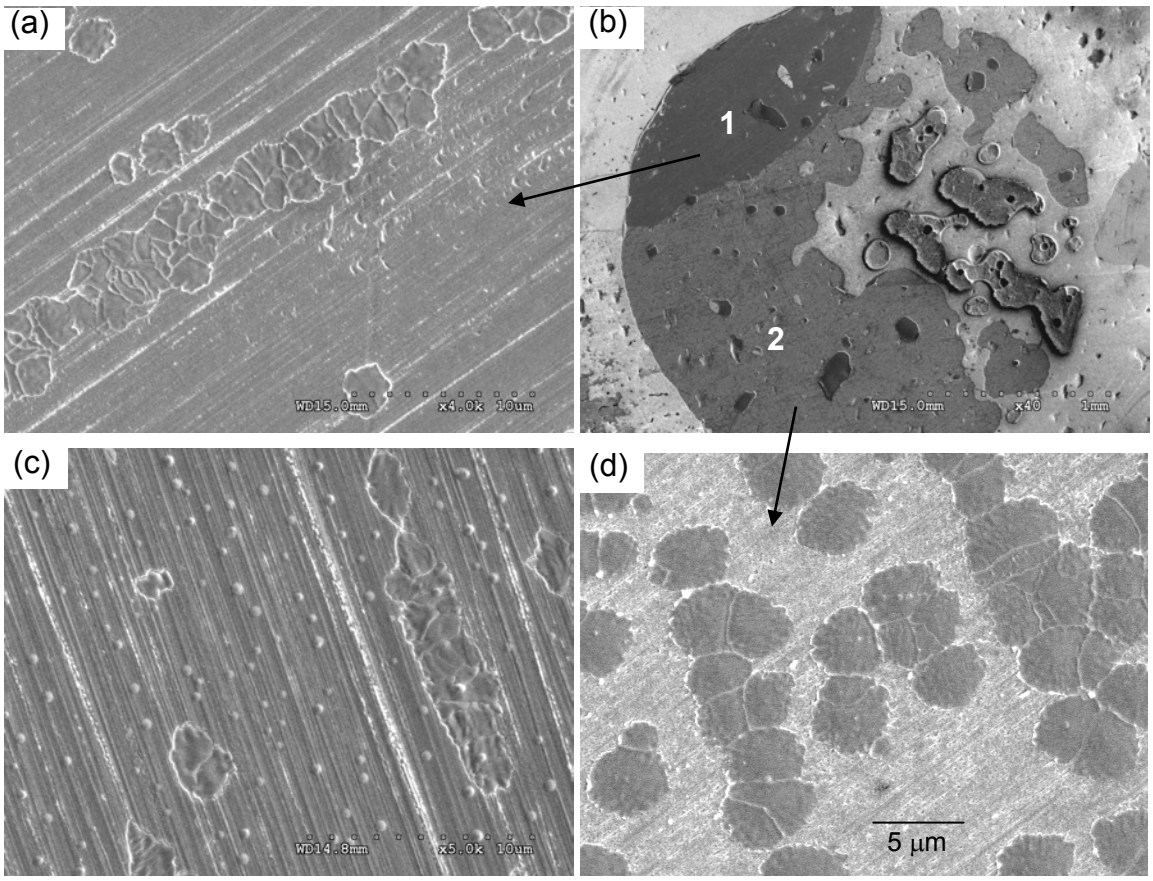

Figure 4: SEM images showing the alloy surface and oxide underside after scale removal. (b) is the specimen surface under a pull stub showing partial failure at the scale/alloy interface exposing two large alloy grains. (a) and (d) are magnified views from grains 1 and 2 respectively, showing different number density of α-Al_2O_3 patches, patch impingement and preferential patch formation along scratch marks. (c) is an image from the underside of the oxide after pulling; small particle like features may be contaminants.

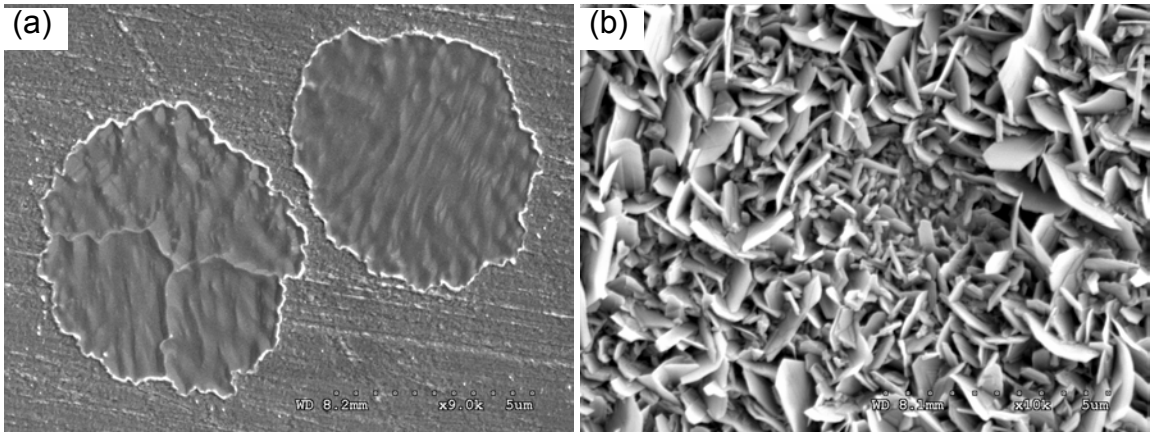

Figure 5: SEM images of (a) two α-Al_2O_3 patches on the alloy surface and (b) platelets and a finer grained patch on the oxide surface.

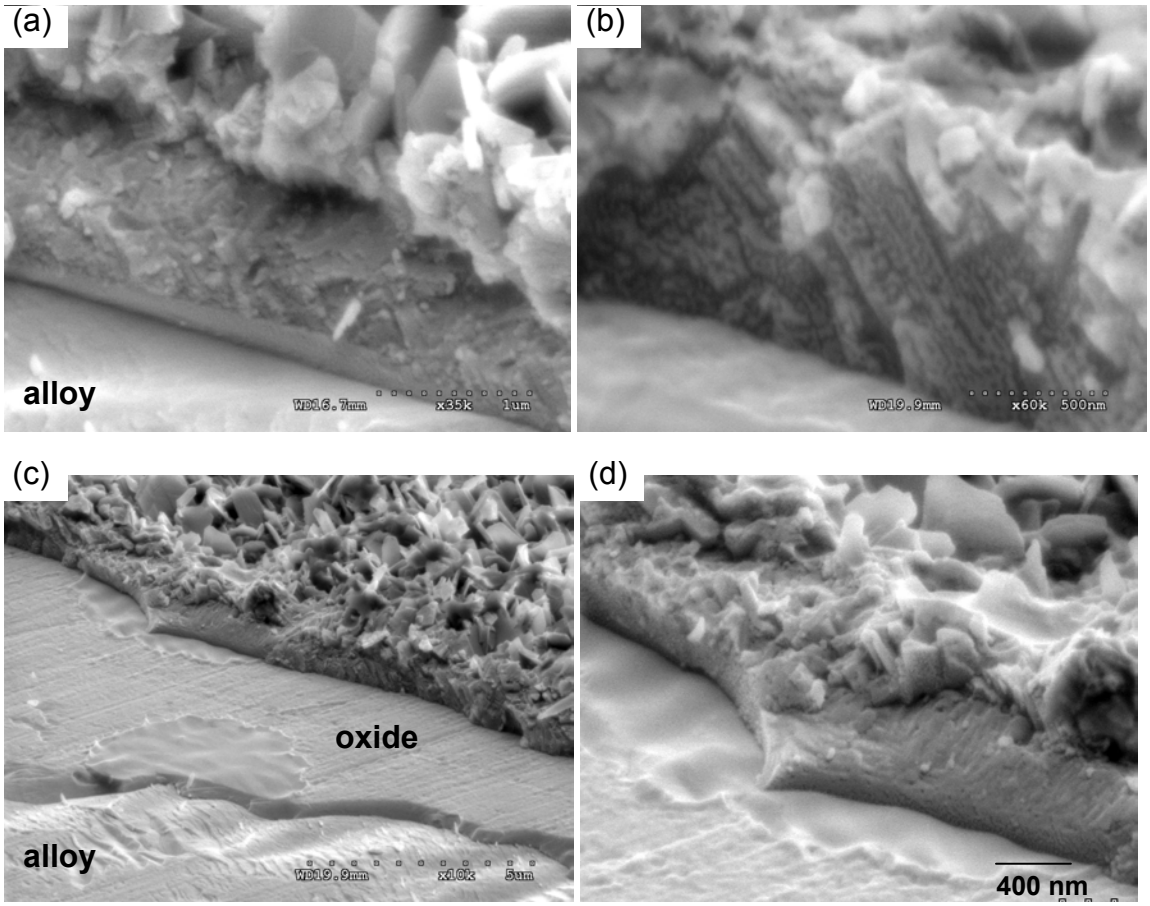

Figure 6: SEM images of (a) fractured scale cross-section showing three structurally different layers of θ-Al_2O_3. (b) Magnified view of the intermediate layer consists of fine, dense platelets. (c) Fractures at oxide/alloy and inner/intermediate layer interfaces showing transformed patches through the inner layer. (d) Magnified view of (c) showing the grain structure above a transformed patch.

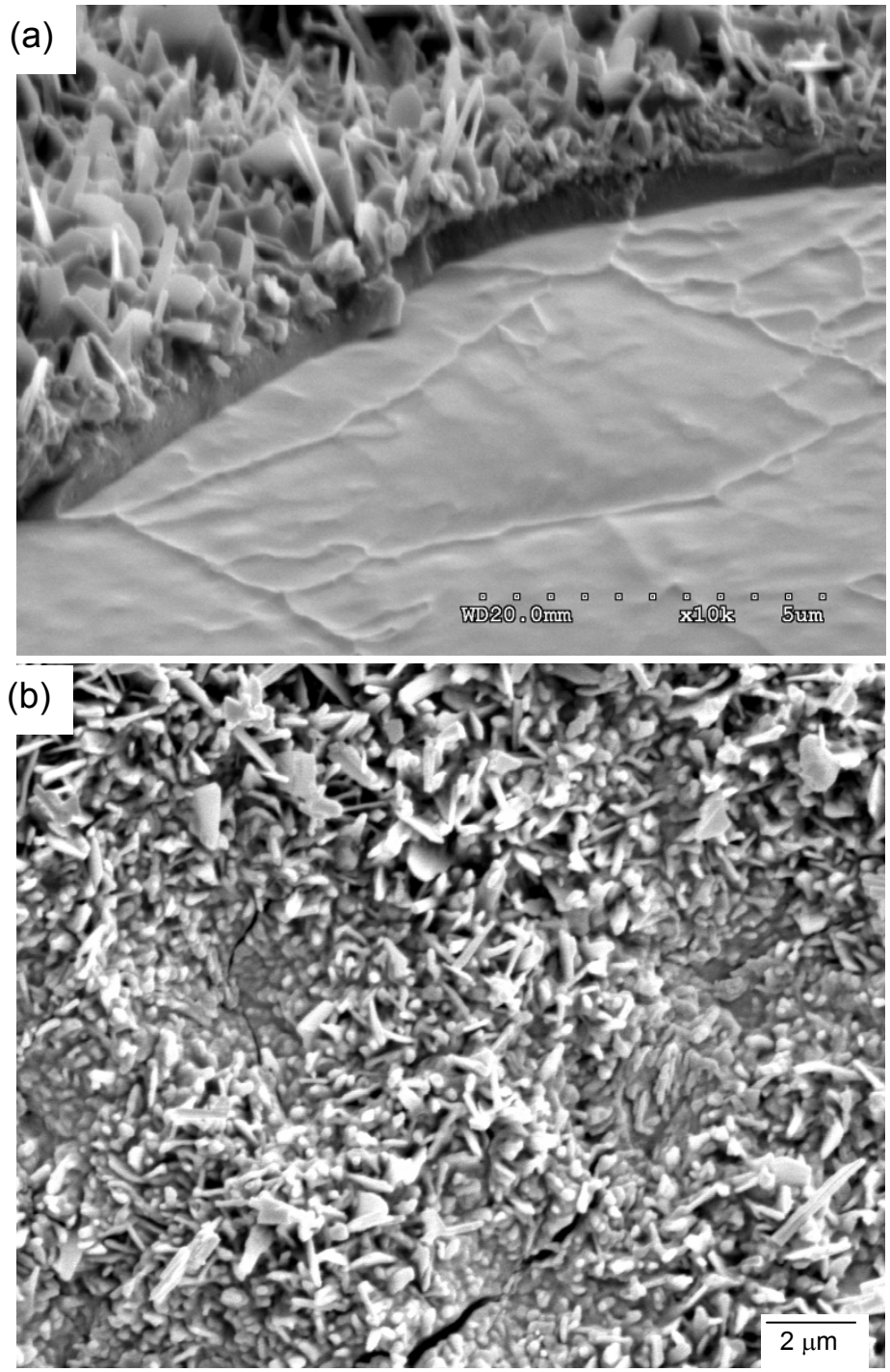

Figure 7: SEM micrographs of scales after the end of the 1000°C strain test, showing (a) scale cross section showing α-Al_2O_3 throughout the inner layers of the first formed theta and large alpha imprints on the alloy. (b) Oxide surface with platelets, dense grained areas and cracks.

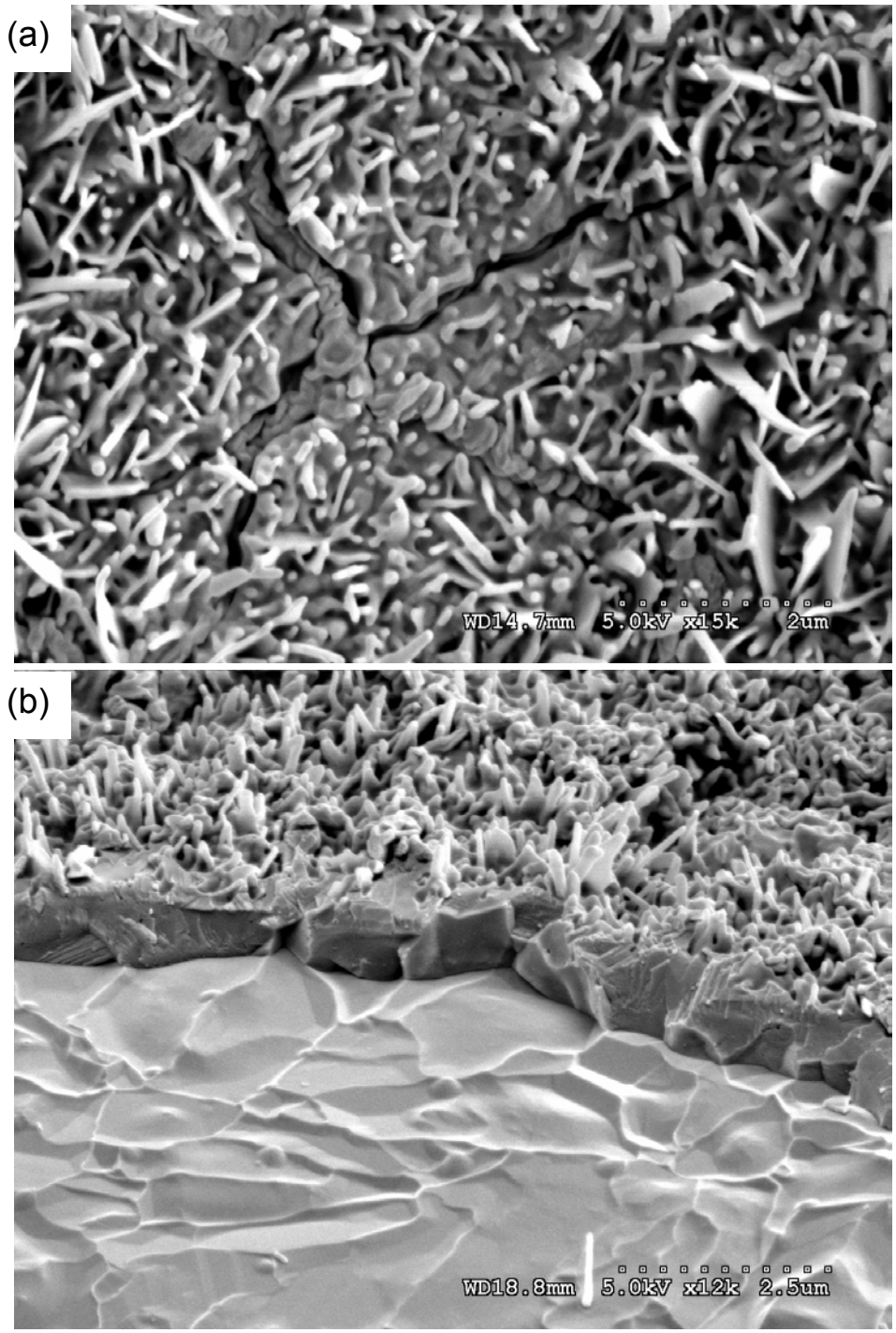

Figure 8: SEM micrographs of scale after the end of the 1100°C strain test, showing (a) surface oxide with platelets, cracks and oxide ridges filling the cracks, and (b) scale x-section and the α-Al_2O_3 imprinted alloy surface.

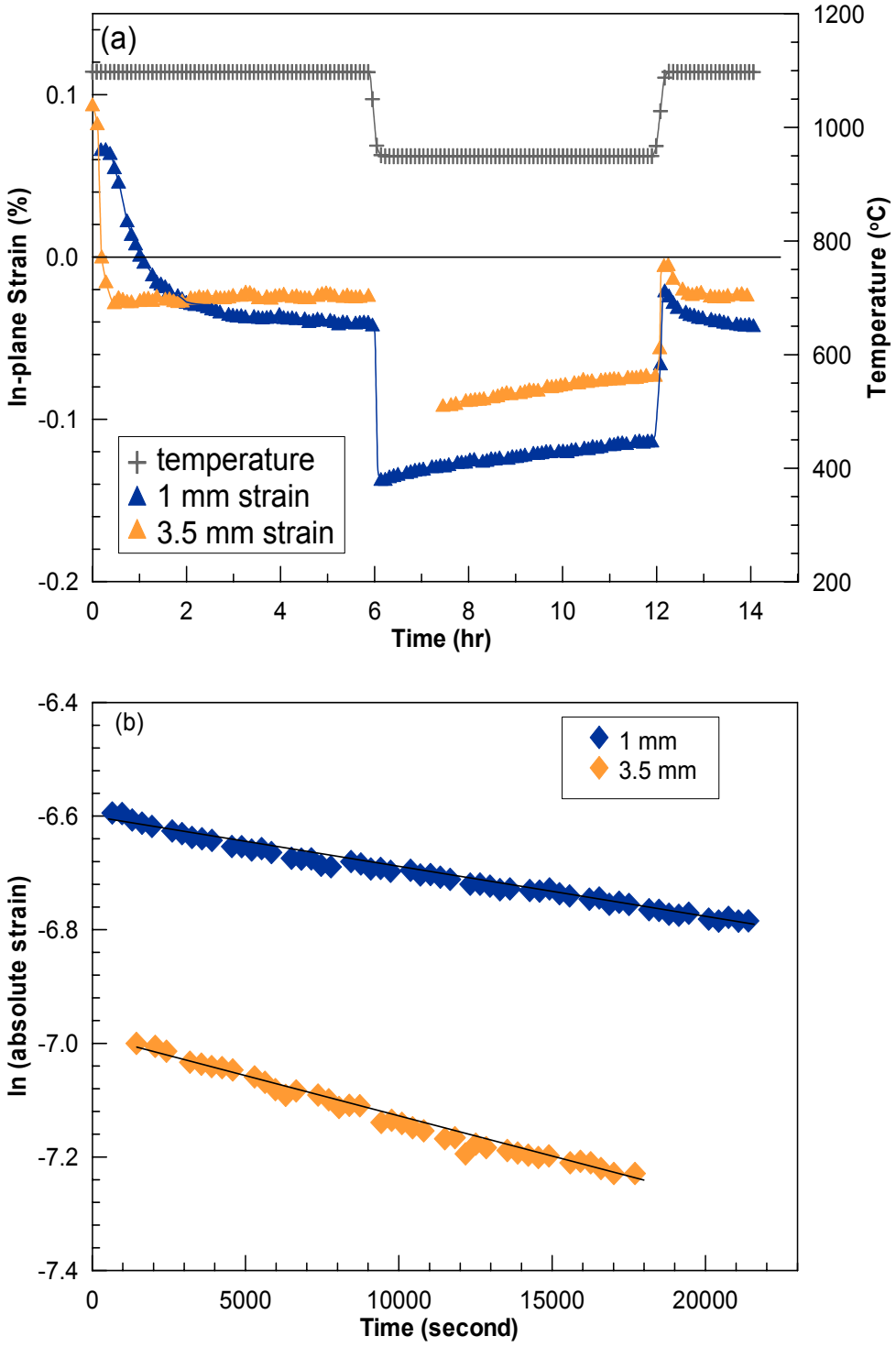

Figure 9: (a) Average strain in α-Al_2O_3 formed on 1 mm and 3.5 mm thick Ni-40Al oxidized at 1100°C, then reduced to 950°C for strain relaxation studies. (b) The change in strain with time at 950°C for the two samples with different substrate thickness; solid lines are linear fits to the data.